Parasitology Research (2019) 118:861–872
https://doi.org/10.1007/s00436-019-06225-w

HELMINTHOLOGY - ORIGINAL PAPER

Identification and characterization of glyceraldehyde 3-phosphate dehydrogenase from *Fasciola gigantica*

Purna B. Chetri[1] · Rohit Shukla[1] · Timir Tripathi[1]

Received: 15 October 2018 / Accepted: 17 January 2019 / Published online: 31 January 2019

Abstract

Fasciola gigantica is an important food-borne trematode responsible for the hepatobiliary disease, commonly known as fascioliasis. In *F. gigantica*, the glyceraldehyde 3-phosphate dehydrogenase (FgGAPDH) is a key enzyme of the glycolytic pathway and catalyzes the reversible oxidative phosphorylation of D-glyceraldehyde-3-phosphate (G-3-P) to 1,3-bisphosphoglycerate (1,3-BPG), with the simultaneous reduction of NAD^+ to NADH. In the present study, we analyzed the sequence of FgGAPDH and investigated its structural, binding, and catalytic properties. Sequence alignment of FgGAPDH showed 100% identity with the sister fluke *Fasciola hepatica* GAPDH. The *gapdh* gene was cloned and expressed in *Escherichia coli*, and the recombinant protein was purified. The purified FgGAPDH exists as a homo-tetramer, composed of a ~ 37-kDa subunit under non-dissociating conditions at 300 mM salt concentration indicating that higher salt stabilizes the tetrameric state. The binding of the cofactor NAD^+ caused a conformational rearrangement in the enzyme structure, leading to the stabilization of the enzyme. A homology model of FgGAPDH was constructed, the cofactor (NAD^+) and substrate (G-3-P) were docked, and the binding sites were identified in a single chain. The inter-subunit cleft of GAPDH that has been exploited for structure-based drug design in certain protozoan parasites is closed in the case of FgGAPDH, similar to the human GAPDH. Thus, the conformation of FgGAPDH in this region is similar to the human enzyme. Therefore, GAPDH may not be a suitable target for drug discovery against fascioliasis. Still, the analysis of the structural and functional attributes of GAPDH will be significant in understanding the various roles of this enzyme in the parasite as well as provide new insights into the biochemistry of flukes.

Keywords *Fasciola gigantica* · Liver fluke · Glyceraldehyde 3-phosphate dehydrogenase · Activity · Modeling · Docking · Quenching

Introduction

Fascioliasis is an economically important food-borne disease of domestic ruminants of the temperate and tropical regions. It is caused by two trematode parasites *Fasciola hepatica* and *Fasciola gigantica* (Cywinska 2005; Mas-Coma et al. 2001). These zoonotic parasites were responsible for a significant economic loss of over US$ 3 billion p.a. in livestock production (Anderson et al. 1999; Elshraway and Mahmoud 2017). Approximately 70% of humans in the temperate countries and around 25–100% of the cattle in Africa, the Middle East, and South-east Asia are infected by these parasites (WHO 2015). The World Health Organization reported that about 2.4–11 million people are infected worldwide with several million at risk (WHO 2015). Humans most often become accidental hosts of *Fasciola* when they ingest the metacercaria encysts present on the aquatic vegetation (Biu et al. 2006).

These parasites require efficient energy production as they constitutively undergo active and continuous growth. Glyceraldehyde-3-phosphate dehydrogenase (GAPDH; EC 1.2.1.12) is the key glycolytic enzyme (Fothergill-Gilmore and Michels 1993). It catalyzes the reversible oxidative phosphorylation of D-glyceraldehyde-3-phosphate (G-3-P) to 1,3-bisphosphoglycerate (1,3-BPG) in the presence of NAD^+ and inorganic phosphate liberating NADH (Harris and Waters 1976). GAPDH is widely distributed in nature ranging from

Section Editor: Xing-Quan Zhu

Electronic supplementary material The online version of this article (https://doi.org/10.1007/s00436-019-06225-w) contains supplementary material, which is available to authorized users.

✉ Timir Tripathi
timir.tripathi@gmail.com; ttripathi@nehu.ac.in

[1] Molecular and Structural Biophysics Laboratory, Department of Biochemistry, North-Eastern Hill University, Shillong 793022, India

bacteria to higher eukaryotes and humans. Most GAPDH have a homo-tetrameric structure, each subunit of molecular mass ~ 35–37 kDa; however, some dimeric and trimeric forms of the enzyme have also been reported (Ashmarina et al. 1981; Carlile et al. 2000; Ferreira-da-Silva et al. 2006). Each subunit of GAPDH contains two binding sites: one for the substrate G-3-P and another for the co-enzyme NAD^+. Additionally, each subunit contains a single catalytic –SH group at the active site that plays a key role in the catalysis. Apart from the role in carbon metabolism, GAPDH is also involved in various other cellular functions (Sirover 1999), including gene regulation (Baxi and Vishwanatha 1995), vesicle transport, nucleic acid binding (Schultz et al. 1996), nuclear RNA export (Singh and Green 1993), apoptosis (Saunders et al. 1999), and neurodegenerative diseases (Mazzola and Sirover 2001); thus, it has been identified as a moonlighting protein.

Certain adenosine derivatives and 1,4-dihydro-4-oxoquinoline ribonucleosides, which target the GAPDH of *Trypanosoma* spp., kill the organisms at micromolar concentrations (Aronov et al. 1999; Soares et al. 2013). Anti-trypanosomal compounds that target GAPDH have also been isolated from *Keetia leucantha* leaves (Bero et al. 2013). 3-Bromopyruvate, an antitumour compound, targets the human GAPDH resulting in altered energy metabolism and cell death (Dell'Antone 2009; Ganapathy-Kanniappan et al. 2009; Ganapathy-Kanniappan et al. 2013). Therefore, inhibition of GAPDH would likely result in reduced energy production and reduced growth of the organism. In this work, we report the cloning of *F. gigantica gapdh* gene as well as the expression, purification, and characterization of the encoded protein.

Materials and methods

The kits for molecular biology and the nickel-nitrilotriacetic acid (Ni^{2+}-NTA) agarose matrix were purchased from Qiagen (CA, USA). Other chemicals and reagents were ordered from Sigma-Aldrich (St. Louis, MO, USA) and Sisco Research Laboratories (Mumbai, India). The media for bacterial culture were purchased from Himedia Laboratories (Mumbai, India). Enzymes and the deoxynucleotide triphosphates (dNTPs) were ordered from New England Biolabs (MA, USA).

Collection of the liver flukes

Fasciola gigantica samples were collected from naturally infected cattles from Bada Bazaar slaughterhouse, Shillong, India, and washed thoroughly with Milli-Q followed by chilled 1× phosphate-buffered saline (PBS, pH 7.4). The flukes were fixed with liquid nitrogen and stored in − 80 °C until use.

RNA isolation and cDNA synthesis

Total RNA isolation was carried out using RNAse easy mini kit (Qiagen), and the first-strand cDNA synthesis was performed using QuantiTect reverse transcription kit (Qiagen).

PCR amplification and cloning of *gapdh*

The full-length *gapdh* gene of *F. gigantica* (1017 bp) was amplified from the cDNA using Phusion High-Fidelity DNA Polymerase and the gene-specific primer pairs having different restriction sites. The sequences of the forward and reverse primers were 5′-GGATCCATGTCCAAACCCAAAGTG-3′ and 5′-AAGCTTTCACAAATGGTCAATAGTATG-3′ having *Bam*HI and *Hind*III restriction sites (underlined), respectively. The following PCR program was used: initial denaturation at 98 °C for 30 s, followed by 30 cycles of amplification consisting of denaturation at 98 °C for 10 s, annealing at 64 °C for 10 s, extension at 72 °C for 25 s, and a final extension of 72 °C for 5 min. The PCR products were resolved using 1% agarose gel electrophoresis in 1× TAE buffer and purified with the QIAquick Gel Extraction Kit (Qiagen). The amplified product was cloned into the pSK+ cloning vector, transformed into *Escherichia coli* DH5α cells. The recombinant plasmids were selected on ampicillin (100 μg mL^{-1}) plates and X-gal and IPTG were added for blue-white screening. The positive plasmids were isolated and screened by restriction digestion, followed by sequence confirmation of the clone. The gene without any mutation was further subcloned into the pET28a(+) expression vector at the defined restriction sites.

Overexpression and purification of FgGAPDH

To check the expression of FgGAPDH, the recombinant FgGAPDH-pET28a(+) construct was transformed into competent *E. coli* $codon^+$ expression cells and plated on LB agar plate supplemented with kanamycin (50 μg mL^{-1}). A single colony was inoculated into 5 mL of LB media containing 50 μg mL^{-1} kanamycin and grown overnight with continuous shaking at 37 °C. This starter culture was used to inoculate 500 mL of LB media containing 50 μg mL^{-1} kanamycin in a 1:100 ratio and grown with continuous shaking at 37 °C until it reached an optical density OD_{600} ~ 0.6–0.8. The culture was then cooled down and induced with 1.0 mM isopropyl β-D-1-thiogalactopyranoside (IPTG) and further grown at 16 °C, with shaking at 150 rpm for 24 h. The cells were harvested by centrifugation at 4 °C, resuspended in ~ 40 mL of equilibration buffer, henceforth called as buffer A (50 mM HEPES pH 7.4, 300 mM NaCl, 10% (*v*/*v*) glycerol) and stored at − 80 °C until use.

Prior to sonication, 1× protease inhibitor cocktail was added to the cell lysate and the cells were lysed in ice

(50 Hz amplitude, 30 s pulse with 30 s interval, 30 cycles). The crude lysate was centrifuged at 13,000 rpm for 30 min at 4 °C. The supernatant was filtered through a 0.45-μm pore size polyvinylidene difluoride (PVDF) membrane before purification by Ni^{2+}-NTA affinity chromatography. The matrix was washed extensively with 10 bed volumes of buffer A. The supernatant was applied to the matrix followed by washing with increasing concentrations of imidazole. The recombinant protein was eluted with the elution buffer (50 mM HEPES pH 7.4, 300 mM NaCl, 10% glycerol, 300 mM imidazole) in three fractions of 2 mL each. The concentration of the purified protein was measured spectrophotometrically by Bradford method using BSA as the standard. The purified protein was analyzed by 12% SDS-PAGE and dialyzed overnight with the dialysis buffer (50 mM HEPES pH 7.4, 300 mM NaCl, 10% glycerol, 2 mM DTT) at 4 °C to remove imidazole.

Determination of molecular mass and subunit status

The native molecular mass of FgGAPDH was determined by gel exclusion chromatography on Superdex™ 200 10/300 GL column (exclusion limit 700 kDa for proteins) on an ÄKTA-FPLC (GE HealthCare Biosciences, USA) under non-dissociating conditions. The column was equilibrated with equilibration buffer (50 mM HEPES pH 7.4 containing 300 mM NaCl and 10% glycerol) at room temperature and loaded with 500 μL of affinity purified FgGAPDH and eluted at a flow rate of 0.3 mL min^{-1}. The protein was detected by its absorbance at 280 nm.

Enzyme activity assays

The enzyme activity of FgGAPDH was measured spectrophotometrically using a Varian Cary 50 UV-Visible spectrophotometer by measuring the increasing in absorption at 340 nm resulting from the reduction of NAD^+ to NADH (Krebs 1955). For the assay, 1 mL reaction mixture containing 100 nM FgGAPDH, 1 mM NAD^+, 20 mM sodium arsenate, and 50 mM HEPES, pH 7.4 was incubated at 37 °C for 15 min. The reaction was started by adding 2 mM G-3-P (stock: 51 mg mL^{-1}) and the absorption was recorded at 10 s intervals for 5 min (Nelson et al. 2001).

The catalytic parameters such as K_m, V_{max}, K_{cat}, and K_{cat}/K_m for G-3-P and NAD^+ were determined by varying the concentration of one ligand while keeping the other constant. Data were fitted through non-linear regression by plotting the Michaelis–Menten graph. Kinetic measurements were performed by the GraphPad Prism 3.0 software. The experiments were performed in triplicates, and the background data was subtracted in all the experiments.

Fluorescence quenching

Quenching of the fluorescence of the tryptophan (Trp) residues of FgGAPDH protein was performed on the Perkin Elmer fluorescence spectrometer LS 55. To 1 μM FgGAPDH, increasing concentrations of the stock quencher solutions of G-3-P (300 mM), NAD^+ (30 mM), acrylamide (10 M), and KI (5 M) were added. The solutions were excited at 280 nm and emission was recorded from 300 to 500 nm using slit width of 5 nm. The Stern–Volmer constant was calculated using the equation

$$F_0/F = 1 + K_{SV}\,[Q]$$

where F is the fluorescence intensity in the presence of quencher, F_0 is the intensity in the absence of quencher, $[Q]$ is the concentration of quencher, and K_{SV} is the Stern–Volmer constant. The dissociation constant (K_d) was calculated by using a plot of fractional change in fluorescence intensity vs quencher concentration.

Phylogenetic analysis

FgGAPDH sequence was submitted to BLAST search to predict the homologs as earlier. From NCBI, 10 homologous sequences were selected and aligned using the ESpript 3.0 software, which utilizes the ClustalW algorithm. Phylogenetic analysis of FgGAPDH was also carried out by ClustalW (Chenna et al. 2003) algorithm by using an online server (https://www.genome.jp/tools-bin/clustalw).

Homology modeling and structure validation

The FgGAPDH sequence was submitted to PDB-BLAST to predict the closely related homologs, and the structure of the GAPDH of *Brugia Malayi* (PDB ID: 4K9D) was selected as the template for homology modeling. The FgGAPDH was aligned with BmGAPDH sequence using the ESpript3.0 server (Robert and Gouet 2014), and a color coded alignment was generated. The structure was modeled on the basis of the crystallographic information of BmGAPDH using MODELLER 9.16 (Webb and Sali 2014). The predicted model was validated by structure alignment using Chimera 1.10.2 (Pettersen et al. 2004), ProSA-web (Wiederstein and Sippl 2007), PDBsum (Laskowski et al. 1997), MetaMQAPII (Pawlowski et al. 2008), ERRAT (Colovos and Yeates 1993), and Verify3d (Bowie et al. 1991; Luthy et al. 1992) servers. ProSA-web was used to calculate the Z score and energy value. PDBsum was used for constructing the Ramachandran plot to visualize the backbone dihedral angles ψ against ϕ of the amino acid residues in the protein structure. MetaMQAPII was used for the prediction of GDT_TS and RMSD, which were calculated by aligning other GAPDH structures available in PDB. If the

GDT_TS and RMSD scores are high and low, respectively, then the structure is acceptable. ERRAT was used to calculate the statistics of non-bonded interactions between different atom types. It calculates the value from highly refined structures. Verify3D was used to determine the compatibility of the 3D atomic model of FgGAPDH with its own amino acid sequence by assigning a structural class based on its location and environment and comparing the results to known structures.

Cavity identification and binding site analysis

After validation, the modeled structure was used for binding site prediction. The binding site was predicted using the PDB structure co-crystallized with substrate and cofactor (Frayne et al. 2009). Chimera1.10.2 was used to visualize the hydrogen bonding, electrostatic and steric interactions. For the identification of the residues, the *E. coli* GAPDH (PDB ID: 2VYV) was retrieved from the PDB database (Frayne et al. 2009) that is co-crystallized with the cofactor and substrate analogs. To predict the binding site of NAD^+ (cofactor) and G-3-P (substrate), the FgGAPDH model was superimposed with EcGAPDH using Chimera1.10.2 (Pettersen et al. 2004). For G-3-P, the key binding site residues Thr178, Thr183, and Arg235 were selected (Frayne et al. 2009), while for NAD^+, Arg13, Ile14, Asp35, Ser126, and Asn317 were selected (Frayne et al. 2009). The binding site cavity associated with these residues was selected for docking.

Molecular docking

The G-3-P and NAD^+ were docked using AutoDock (Goodsell et al. 1996). AutoDock is a freely available and extensively used software for protein-ligand docking (Pathak et al. 2017). AutoDock uses the semi-empirical free energy force field for the calculation of ligand binding conformations. The FgGAPDH structure and ligands (substrate and cofactor) were prepared using AutoDock 1.5.6. Hydrogen atoms were added to the structure of FgGAPDH, and partial atomic charges were assigned. A 3D grid box for docking was set into $X = 50°$, $Y = 42°$, $Z = 46°$ grid points, and the grid spacing was 0.398 Å for G-3-P. For NAD^+, the 3D grid box was set into $X = 58°$, $Y = 68°$, $Z = 72°$ grid points, and the grid spacing was 0.452 Å. The binding poses were generated by Lamarckian genetic algorithm. Other docking parameters were population size (150), maximum number of evaluations (25.00,000), maximum number of generations (27,000), rate of gene mutation (0.02), and rate of crossover (0.8). All other parameters were kept as default. Two thousand binding poses were generated for each ligand. The results were clustered according to the RMSD values and ranked by the binding free energy.

Results

Multiple sequence alignment and phylogenetic analysis of FgGAPDH

The BLAST tool from NCBI was used to identify the closely related homologs of FgGAPDH. The protein BLAST of FgGAPDH resulted in two putative domains, N-terminal NAD^+ binding domain (residues 1–150) and C-terminal substrate binding domain (residues 151–338). We retrieved 10 sequences from various species for phylogenetic analysis (*Fasciola hepatica*, *Opisthorchis viverrini*, *Schistosoma haematobium*, *Schistosoma mansoni*, *Schistosoma japonicum*, *Echinococcus multilocularis*, *Haemonchus contortus*, *Brugia malayi*, *Onchocerca volvulus*, and *Homo sapiens*) to identify and compare the conserved residues and their evolutionary relatedness with FgGAPDH. Interestingly, the amino acid sequence of FgGAPDH showed 100% sequence identity with the GAPDH of *F. hepatica*. From pairwise sequence alignment, it was observed that the sequence FgGAPDH showed high sequence similarity with related organisms, such as *O. viverrini* (86.69%), *S. japonicum* (77.22%), *S. haematobium* (76.33%), *S. mansoni* (76.63%), *B. malayi* (74.41%), *O. volvulus* (73.53%), *E. multilocularis* (72.40%), and *H. contortus* (69.01%). It also showed 70.54% sequence identity with *H. sapiens* (Fig. 1).

Multiple sequence alignment revealed several conserved residues and conserved motifs that are important for the catalytic activity of GAPDH. Sequence motifs like ^{12}GRIGRLV^{18}, ^{34}NDPFI^{38}, ^{122}ISAPS^{126}, and ^{314}WYDNE^{318} that are reported to be important for NAD^+ binding (Baker et al. 2014; Frayne et al. 2009; Jenkins and Tanner 2006) were conserved. They form the hydrophobic core as well as contain the catalytic residues and make a novel binding cavity for cofactor stabilization. These motifs are also conserved in humans. The substrate binds to the active site and converts to product by a mechanism using NAD^+. The motifs ^{173}EGLMTT^{178}, ^{183}TATQ^{186}, and ^{235}RVPT^{238} serve as the catalytic core for substrate stabilization (Frayne et al. 2009) and are the key residues that are required for the catalytic activity. Several other residues are also conserved that facilitate cofactor and substrate binding. The conserved residues and motifs that are involved in substrate and NAD^+ binding are highlighted in the Fig. 1.

The evolutionary relationship with FgGAPDH was studied based on the comparison of all the 10 retrieved sequences (Fig. 2). FgGAPDH and OvGAPDH were closely related because they originate from the same clade as FgGAPDH and FhGAPDH. They also showed the highest sequence similarity in pairwise alignment. All *Schistosoma* species sequences originated from the same clade and share similar evolutionary pattern but they differed from FgGAPDH. Sequences of *H. contortus*, *B. malayi*, and others originated from other clades.

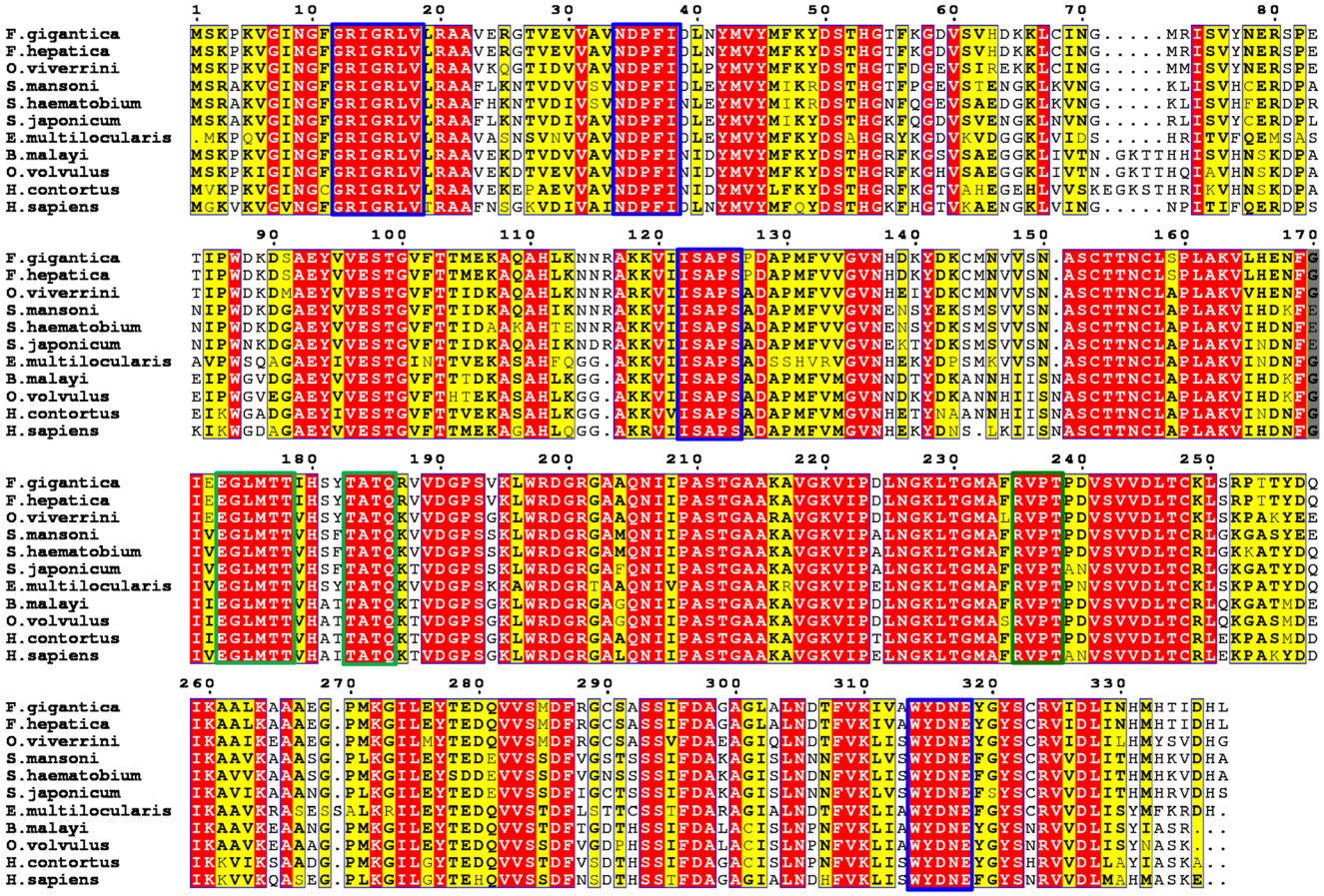

Fig. 1 Multiple sequence alignment. Alignment of FgGAPDH with GAPDH from related organisms and human. The alignment was generated by ClustalW algorithm. *Fasciola hepatica* (AIE44418.1), *Opisthorchis viverrini* (009169164.1), *Schistosoma haematobium* (012801387.1), *Schistosoma mansoni* (CCD75626.1), *Schistosoma japonicum* (CAX80276.1), *Echinococcs multilocularis* (AAA61574.1), *Haemonchus contortus* (ADI46817.1), *Brugia malayi* (001899849.1), *Onchocerca volvulus* (CAA70607.1), and *Homo sapiens* (AAH83511.1) were included in the alignment. Similar residues are shown in yellow boxes; the red boxes represent identical amino acid residues while the amino acid residues with different properties have no boxes. Blue boxes represent NAD^+ binding site while green boxes represent G-3-P binding conserved motifs

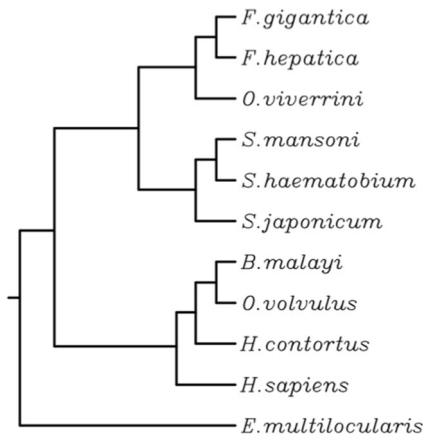

Fig. 2 Phylogenetic relation of the FgGAPDH with other related organisms and human. The NJ method was used to construct the phylogenetic tree by comparing amino acid sequences. Tree describes the evolutionary relationship between different organisms

HsGAPDH showed far-related evolutionary relationship with FgGAPDH though it showed 70.54% sequence similarity, suggesting that the HsGAPDH is evolutionary far from the FgGAPDH.

Cloning, overexpression, and purification of FgGAPDH

The *F. gigantica gapdh* gene (1071 bp) was amplified and the PCR product was cloned into pSK+ vector followed by blue-white screening to confirm the positive clone. The positive clone was further confirmed by restriction digestion using defined restriction enzymes. Upon digestion, two bands ~ 1.0 kb (*gapdh* gene) and ~ 2.9 kb (pSK+ vector backbone) were obtained (Supplementary Figure 1). The sequence fidelity of the positive clone was further confirmed by sequencing.

The digested gene fragment was cloned into the pET28a(+) expression vector and confirmed by digestion.

FgGAPDH is composed of 338 amino acid residues with a calculated molecular mass of ~ 37 kDa and a theoretical pI value of 7.10. The FgGAPDH protein was highly expressed and predominantly (> 95%) present in the soluble fraction. The yield of purified FgGAPDH was ~ 18 mg L^{-1}. The purified FgGAPDH was homogenous as indicated by a single protein band on SDS-PAGE (Fig. 3a).

FgGAPDH exists as homo-tetramer in solution

The oligomeric status and molecular mass of the purified recombinant FgGAPDH were determined under non-dissociating conditions at 300 mM NaCl concentration using size exclusion chromatography (SEC). Gel filtration of FgGAPDH on a Superdex S-200 column showed a single peak with an elution volume of 13.4 mL (Fig. 3b) that corresponds to about 145 ± 5 kDa when compared with the molecular weight markers. The results of the SDS-PAGE along with SEC suggest that FgGAPDH exists as a tetramer under non-dissociating conditions.

Kinetic analysis of FgGAPDH

The steady-state kinetics of FgGAPDH with G-3-P and NAD^+ were calculated using the Michaelis–Menten plot as shown in Fig. 4 and Table 1. The calculated kinetic parameters of FgGAPDH fall within the previously reported range of FhGAPDH (Zinsser et al. 2014). Under our experimental conditions, the K_m of FgGAPDH was found to be slightly higher than FhGAPDH. The comparative analysis of the kinetic parameters of FgGAPDH and the FhGAPDH is shown in Table 1.

Binding affinity of GAPDH towards the substrate (G-3-P) and cofactor (NAD^+)

Fluorescence quenching is an important method to determine the binding affinity of substrates, cofactors, and other ligands with a protein. A subtle change in the microenvironment of the buried Trp residues upon ligand binding can be detected as a factor of change in fluorescence intensity.

To understand how the binding of G-3-P and NAD^+ influences the Trp microenvironment in FgGAPDH, intrinsic Trp fluorescence quenching was performed. A decrease in the intensity of fluorescence emission was observed upon binding of FgGAPDH and G-3-P or NAD^+, suggesting binding of the quencher near the solvent accessible Trp residues. From the quenching experiment, the Stern–Volmer plot was constructed to obtain the Stern–Volmer constant (K_{sv}). The K_{sv} value for G-3-P and NAD^+ was found to be 0.278×10^{-3} μM^{-1} and 19.5×10^{-3} μM^{-1}, respectively (Fig. 5a, b). The fractional change in the fluorescence intensity vs the concentration of G-3-P or NAD^+ suggests a binding constant (K_d) of 0.963 mM and 0.104 mM for G-3-P and NAD^+, respectively (Fig. 5c, d).

NAD^+ binding affects Trp accessibility and stability of the protein

Acrylamide is a neutral fluorescence quencher that can penetrate into the core of protein, whereas KI being ionic in nature can quench only the surface lying Trp residues (France and

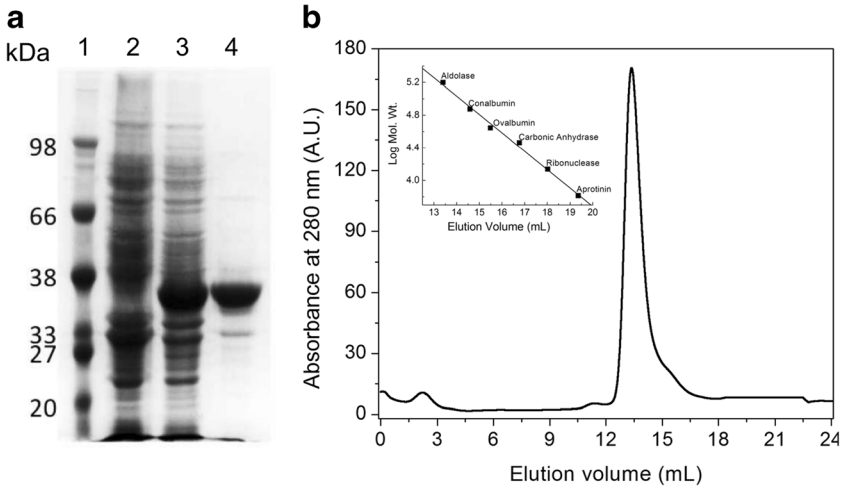

Fig. 3 Overexpression of FgGAPDH in *E. coli* and purification of the recombinant protein on Ni-NTA agarose. **a** SDS-PAGE analysis of cell lysate showing overexpression of FgGAPDH and the purified protein. Lanes 1–4 represent molecular weight markers, supernatant of uninduced culture lysate, supernatant of induced culture lysate, and purified protein, respectively. **b** Molecular mass and subunit structure of FgGAPDH. SEC profile of FgGAPDH on Superdex™ 200 10/300 GL column. The inset shows the column calibration curve. The column was calibrated with the gel filtration calibration kit containing aldolase (158 kDa), conalbumin (75 kDa), ovalbumin (44 kDa), carbonic anhydrase (29 kDa), ribonuclease (13.7 kDa), and aprotinin (6.5 kDa)

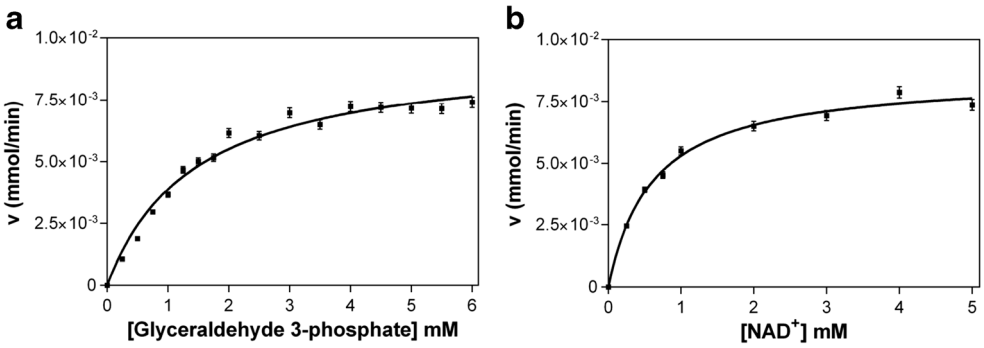

Fig. 4 Michaelis–Menten plots. Enzymatic activities were measured at various concentrations of glyceraldehyde 3 phosphate (**a**) and NAD^+ (**b**). Kinetic constants were obtained using the Graph Pad Prism software. Results are mean ± S.D. of three independent measurements

Grossman 2000; Möller and Denicola 2002; Van de Weert and Stella 2011). FgGAPDH contains 12 Trp residues in its native tetrameric structure. Fluorescence quenching of FgGAPDH with these quenchers was performed with and without the cofactor NAD^+ (further designated as holo-FgGAPDH and apo-FgGAPDH, respectively), to understand the role of NAD^+ in the structural dynamics of the protein.

Upon binding of acrylamide, a decrease in the fluorescence intensity was observed for both apo- and holo-FgGAPDH. The K_{sv} was higher for the apo-FgGAPDH (3.33×10^{-3} μM^{-1}) compared to the holo-FgGAPDH (0.93×10^{-3} μM^{-1}), suggesting higher affinity of acrylamide for apo-FgGAPDH (Fig. 6a); thus, the presence of NAD^+ confers additional conformational stability to the holo-FgGAPDH. Similarly, during KI quenching, there was a decrease in the fluorescence intensity for both holo- and apo-FgGAPDH and the affinity of KI was also found to be higher for the apo-FgGAPDH (1.06×10^{-3} μM^{-1}) in comparison to the holo-FgGAPDH (0.38×10^{-3} μM^{-1}) (Fig. 6b), suggesting that NAD^+ causes conformational rearrangement in the holo-FgGAPDH and the Trp residues become less accessible to the quencher. A smaller K_{sv} for KI quenching in comparison to that of acrylamide could be due to the inability of KI to access the Trp residues present in the interior of the protein due to its ionic nature. The Stern–Volmer constant (K_{sv}) of FgGAPDH for different quencher is shown in Table 2.

Homology modeling and structural validation

The secondary structure of FgGAPDH was predicted by using the PSIPRED server. The structure contains 7 α-helices, 15 β-sheets, and 23 coil conformations (Supplementary Figure 2). The result of BLASTp search revealed many templates with high sequence identity. We used the structure of NAD^+ bound BmGAPDH (PDB ID: 4K9D, X-ray, 2.1 Å) for modeling as it showed the highest identity and query coverage. It showed 72.1% identical and 81.5% similar residues in pairwise alignment (Supplementary Figure 3). Eight models were predicted by MODELLER 9.16, and the best model was selected. To predict the reliability of the predicted model, the model was aligned with BmGAPDH that gave an RMSD value of 0.229 Å for 239 Cα atoms (Fig. 7). The *Z* score, calculated using the ProSA-web server, was within the X-ray crystal structure range and showed a value of − 9.14 for the predicted FgGAPDH model and − 10.7 for the template BmGAPDH structure (Supplementary Figure 4). The energy plot suggested that all the residues had low energy except a few residues (Supplementary Figure 5). Ramachandran plot revealed that 92.6%, 6.4%, 0.7%, and 0.3% residues were in the most favored regions, additional allowed regions, generously allowed regions and disallowed regions, respectively (Supplementary Figure 6). The ERRAT showed a good score of 85.45 (Supplementary Figure 7) and the Verify3D score was found to be 91.72 (Supplementary Figure 8). Alignment of the FgGAPDH structure with the other similar structures using the MetaMQAPII server gave GDT_TS and RMSD values of 47.855 and 3.892 Å, respectively, which is an excellent score, indicating that our structure is acceptable. Thus, all the stereochemical parameters suggested that the modeled structure is good in terms of stereochemical parameters and can be considered for further docking studies.

Table 1 Comparative kinetic parameters of FgGAPDH and FhGAPDH

Organism	K_m G-3-P (mM)	K_m NAD^+ (mM)	V_{max} (μmol s^{-1})	K_{cat} G-3-P (s^{-1})	K_{cat} NAD^+ (s^{-1})	K_{cat}/K_m G-3-P (s^{-1} mM^{-1})	K_{cat}/K_m NAD^+ (s^{-1} mM^{-1})
F. gigantica	1.44 ± 0.26	0.612 ± 0.050	0.158 ± 0.004	1.58 ± 0.07	1.43 ± 0.08	1.10 ± 0.04	2.33 ± 0.11
F. hepatica	1.01 ± 0.15	n.d.	0.044 ± 0.002	n.d.	n.d.	n.d.	n.d.

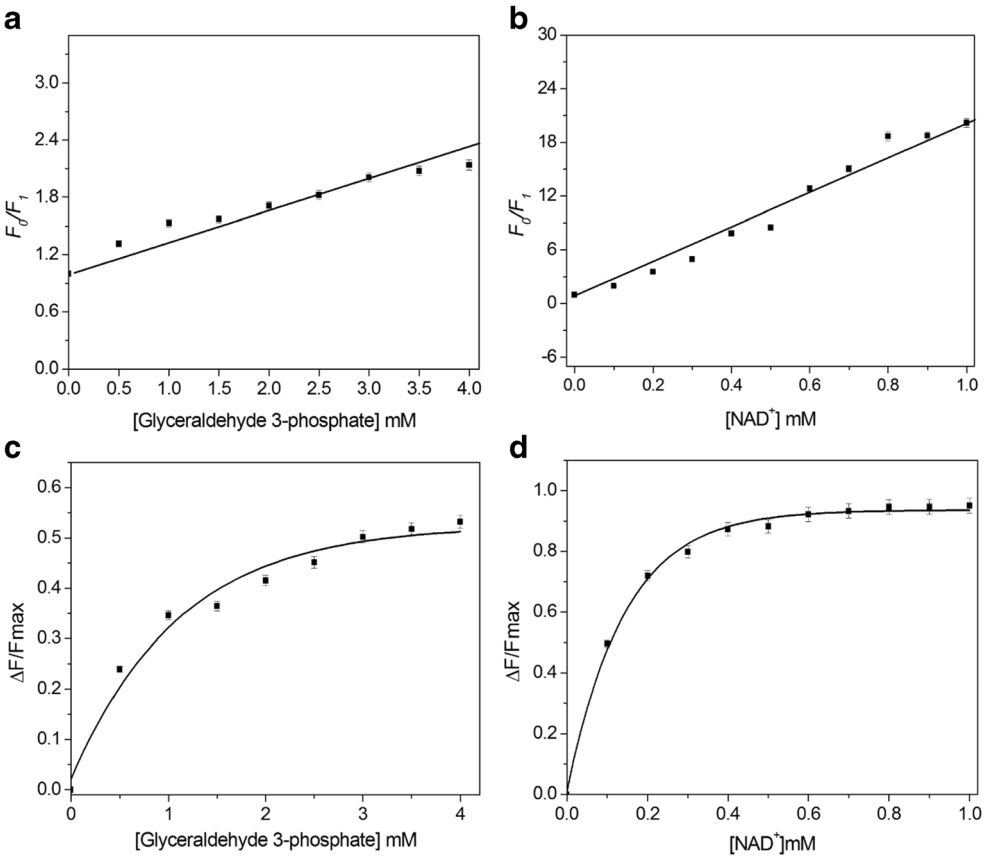

Fig. 5 Fluorescence quenching experiments. The graph is plotted between F_0/F against the concentration of substrate (G-3-P) and cofactor (NAD^+). The straight line shows the quenching of FgGAPDH in the presence of G-3-P (**a**) and NAD^+ (**b**). The Stern–Volmer constant was calculated for both the substrate and cofactor. The K_d was also calculated for both the G-3-P (**c**) and the NAD^+ (**d**)

Molecular docking with substrate and cofactor

Molecular docking is a widely used method to identify the position and orientation of the ligand with respect to the receptor. It helps in the identification of the key interacting residues as well as to predict the protein-ligand binding pattern (Shukla et al. 2017a; Shukla et al. 2017b; Shukla et al. 2018). Here, we docked the G-3-P (substrate) and NAD^+ (cofactor) with the modeled FgGAPDH structure using AutoDock, which showed novel binding patterns and similar interacting residues (Fig. 8).

The binding affinity of NAD^+ was − 6.79 kcal mol^{-1} for FgGAPDH. The complex was stabilized with eight hydrogen bonds with various catalytic residues. Several residues actively participated in the hydrogen bond interactions; they are Arg13 (2.4 Å), Ile14 (2.0 Å), Ser123, (two bonds, 1.996, and 1.928 Å), Cys153 (3.7 Å), Arg80 (2.0 Å), Ser98 (2.1 Å), and Ser 152 (1.8 Å). The residues Asn9, Gly10, Gly12, Asn34, Asp35, Pro36, Phe37, Thr99, Val101, Ala124, and Thr154 actively participated in the hydrophobic interactions.

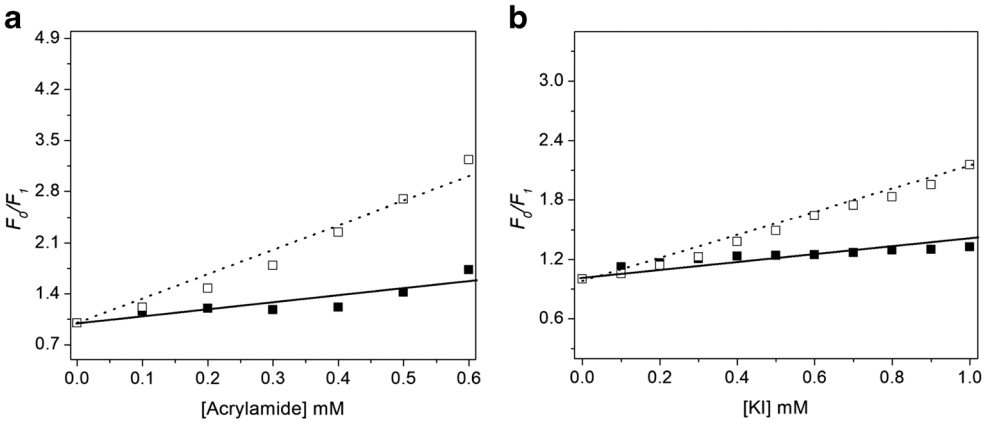

Fig. 6 Quenching of FgGAPDH with acrylamide and KI. The plots shows the quenching of FgGAPDH with acrylamide (**a**) and KI (**b**), in the absence of NAD^+ (unfilled square) and in the presence of NAD^+ (filled square)

Table 2 Stern–Volmer constants (K_{sv}) of FgGAPDH in $\times 10^{-3}$ μM^{-1}

Quenchers	FgGAPDH	FgGAPDH with NAD^+
G-3-P	0.28 ± 0.01	n.d.
NAD^+	19.50 ± 0.92	n.d.
Acrylamide	3.33 ± 0.07	0.93 ± 0.03
KI	1.06 ± 0.03	0.38 ± 0.01

The substrate G-3-P was also docked for predicting the binding pattern of substrate with the FgGAPDH enzyme. The binding affinity was −3.4 kcal mol^{-1} for FgGAPDH. The complex was stabilized with six hydrogen bonds with various catalytic residues. Several residues actively participated in the hydrogen bond interactions; they are Lys195 (1.787 Å), Asp199 (three H-bonds, 1.735, 1.857, and 2.127 Å), and Arg235 (two bonds, 1.852 and 2.471 Å). The residues Thr185, Leu196, and Ala210 actively participated in the hydrophobic interactions.

Discussion

FgGAPDH showed 100% amino acid sequence identity with FhGAPDH, suggesting evolutionary conservation of the protein in the genus. Zinsser et al. have reported the biochemical characterization of recombinant FhGAPDH (Zinsser et al. 2014). They showed that in the absence of ligands, FhGAPDH exists as a mixture of homodimers and tetramers. The addition of either NAD^+ or G-3-P shifted this equilibrium towards a dimeric state. They also demonstrated that the dimeric form was comparatively more stable than the tetrameric form. These responses to ligand binding that leads to alterations in the oligomeric state differ from mammalian GAPDH, which may be exploited for drug discovery. However, it has been reported that the oligomeric states of several mammalian GAPDH can be differentially modulated by ligands. Rabbit GAPDH dissociated into dimers in the presence of NAD^+ and G-3-P (Hoagland Jr. and Teller 1969). In contrast, in some mammalian species, the addition of NAD^+ stabilized the tetrameric state of the enzyme (Lakatos and Zavodsky 1976; Osborne and Hollaway 1976). Thus, the differential existence of oligomeric states, depending on the ligands, may not be suitable for drug discovery against *Fasciola*. We showed the ligand-mediated regulation of the oligomeric structure, but the relevance of this regulation is limited to its utilization for structure-based drug discovery. We observed that at a slightly higher salt concentration (300 mM), the FgGAPDH protein exists in a homogenous tetrameric state and the dimeric population was absent, suggesting that the presence of high salt concentration leads to the association of dimers into tetramers. Therefore, it can be concluded that higher salt concentration stabilizes the tetrameric population of FgGAPDH. The binding affinity of GAPDH for NAD^+ was found to be higher than G-3-P, suggesting stronger interactions between the protein and the cofactor. Using fluorescence quenching studies, we show that binding of NAD^+ confers additional conformational stability to the FgGAPDH.

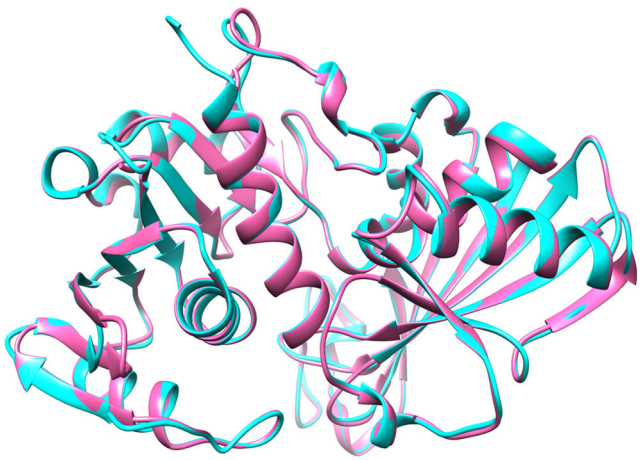

Fig. 7 Structural features of FgGAPDH. Structural alignment of FgGAPDH (cyan) with BmGAPDH (pink) generates 0.229 Å for 239 Cα atoms. Low RMSD value indicates higher structural similarity

The overall architecture of GAPDH is well conserved. It exists as homotetramer consisting of dimer of dimers with known regions of dimerization. Each subunit is composed of ~330 amino acid residues and consists of two domains: an NAD^+ binding domain (residues 1–150) displaying the characteristic Rossmann-fold (a central parallel β-sheet surrounded by α-helices) and a catalytic domain (residues 151–316), containing eight-stranded antiparallel β-sheet and four α-helices. GAPDH is an attractive target for drug discovery against protozoan parasites that live in blood and depend solely on glycolysis for energy production. The inter-subunit cleft present in close proximity to the 2′-OH on the NAD^+ in *Trypanosoma* GAPDH has been exploited for structure-based design of anti-trypanosomatid compounds, particularly adenosine analogues. This cleft is closed in human GAPDH, and the side chain of Ile37 is present, thereby leading to the selectivity of the drugs for the parasite enzyme over the human counterparts. The Ile37 is conserved in FgGAPDH and FhGAPDH (as Ile38), and thus the conformational topology in this region is similar to the human enzyme. Therefore, GAPDH may not be a suitable target for drug discovery against fascioliasis.

Metabolic pathways that extract energy from the carbon-based compounds are essential for energy generation and thus critical for the organism's survival. GAPDH catalyzes one of the two steps of glycolysis that produce NADH. This reaction

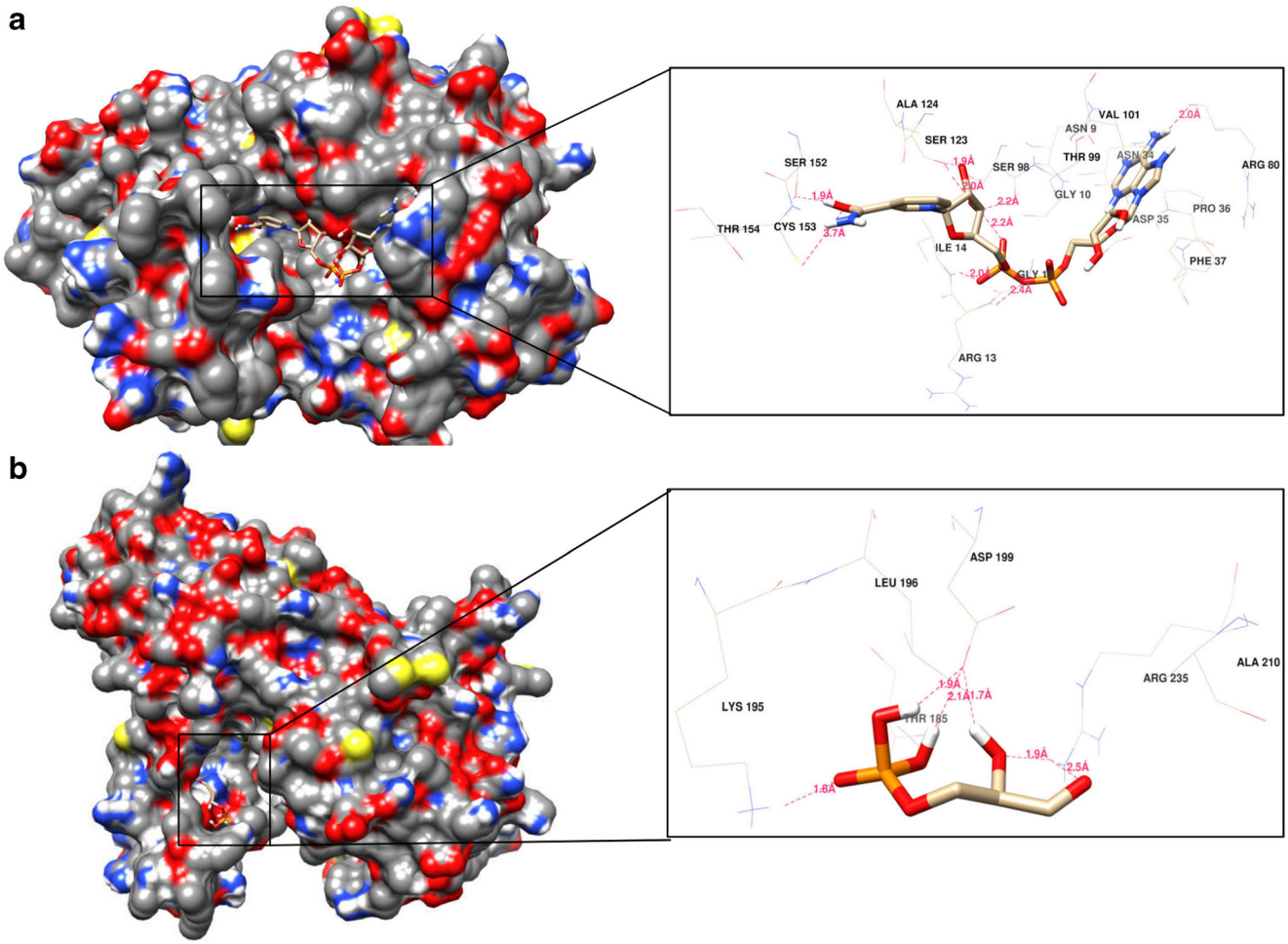

Fig. 8 The potential binding pose for G-3-P and NAD^+. (A) Surface view of G-3-P docked with FgGAPDH. The zoom region shows the residue interaction network with the G-3-P. (B) Surface view of NAD^+ docked with FgGAPDH. The zoom region shows the residue interaction network with the NAD^+. Both ligands are shown in stick form and residues are shown in wire form. The red dotted line represents intermolecular hydrogen bond interactions

precedes the two ATP-generating steps. Thus, the inhibition of GAPDH will lead to significant reduction in energy generation, thereby representing a potential therapeutic strategy to combat the parasitic infections. However, high structural similarity between the host and liver fluke enzymes makes this approach theoretically challenging. Nevertheless, the identification of specific inhibitors of GAPDH from other parasites suggests that slight differences in structural and biochemical properties could be exploited in the development of novel, parasite-specific inhibitors. Nevertheless, the study of the structural and catalytic characteristics of GAPDH will be important in understanding the functions of this enzyme in the parasite as well as provide new insights into the biochemistry of flukes.

Authors' contributions PBC and RS carried out all the experiments. PBC, RS, and TT analyzed the data, conceived the study, and participated in its design and coordination and drafted the manuscript. All authors read and approved the final manuscript.

Compliance with ethical standards

Competing interests The authors declare that there are no competing interests.

Abbreviations GAPDH, Glyceraldehyde 3-phosphate dehydrogenase; FgGAPDH, *F. gigantica* glyceraldehyde 3-phosphate dehydrogenase; SEC, Size exclusion chromatography; G-3-P, D-glyceraldehyde-3-phosphate; DTT, Dithiothreitol; HEPES, (4-(2-Hydroxyethyl)-1-piperazineethanesulfonic acid)

Publisher's Note Springer Nature remains neutral with regard to jurisdictional claims in published maps and institutional affiliations.

References

Anderson N, Luong TT, Vo NG, Bui KL, Smooker PM, Spithill TW (1999) The sensitivity and specificity of two methods for detecting Fasciola infections in cattle. Vet Parasitol 83(1):15–24

Aronov AM, Suresh S, Buckner FS, van Voorhis WC, Verlinde CLMJ, Opperdoes FR, Hol WGJ, Gelb MH (1999) Structure-based design

of submicromolar, biologically active inhibitors of trypanosomatid glyceraldehyde-3-phosphate dehydrogenase. Proc Natl Acad Sci U S A 96(8):4273–4278
Ashmarina LI, Muronetz VI, Nagradova NK (1981) Immobilized D-glyceraldehyde-3-phosphate dehydrogenase can exist as a trimer. FEBS Lett 128(1):22–26
Baker BY, Shi W, Wang B, Palczewski K (2014) High-resolution crystal structures of the photoreceptor glyceraldehyde 3-phosphate dehydrogenase (GAPDH) with three and four-bound NAD molecules. Protein Sci 23(11):1629–1639
Baxi MD, Vishwanatha JK (1995) Uracil DNA-glycosylase/glyceraldehyde-3-phosphate dehydrogenase is an Ap4A binding protein. Biochemistry 34(30):9700–9707
Bero J, Beaufay C, Hannaert V, Herent MF, Michels PA, Quetin-Leclercq J (2013) Antitrypanosomal compounds from the essential oil and extracts of Keetia leucantha leaves with inhibitor activity on Trypanosoma brucei glyceraldehyde-3-phosphate dehydrogenase. Phytomedicine 20(3–4):270–274. https://doi.org/10.1016/j.phymed.2012.10.010
Biu AA, Ahmed MI, Mshelia SS (2006) Economic assessment of losses due to parasitic diseases common at the Maiduguri abattoir, Nigeria. vol 7, p 143–145
Bowie JU, Luthy R, Eisenberg D (1991) A method to identify protein sequences that fold into a known three-dimensional structure. Science 253(5016):164–170
Carlile GW, Chalmers-Redman RM, Tatton NA, Pong A, Borden KE, Tatton WG (2000) Reduced apoptosis after nerve growth factor and serum withdrawal: conversion of tetrameric glyceraldehyde-3-phosphate dehydrogenase to a dimer. Mol Pharmacol 57(1):2–12
Chenna R, Sugawara H, Koike T, Lopez R, Gibson TJ, Higgins DG, Thompson JD (2003) Multiple sequence alignment with the Clustal series of programs. Nucleic Acids Res 31(13):3497–3500
Colovos C, Yeates TO (1993) Verification of protein structures: patterns of nonbonded atomic interactions. Protein Sci 2(9):1511–1519
Cywinska A (2005) Epidemiology of fascioliasis in human endemic areas. J Helminthol 79(3):207–216
Dell'Antone P (2009) Targets of 3-bromopyruvate, a new, energy depleting, anticancer agent. Med Chem 5(6):491–496
Elshraway NT, Mahmoud WG (2017) Prevalence of fascioliasis (liver flukes) infection in cattle and buffaloes slaughtered at the municipal abattoir of El-Kharga, Egypt. Vet World 10(8):914–917. https://doi.org/10.14202/vetworld.2017.914-91
Ferreira-da-Silva F, Pereira PJB, Gales L, Roessle M, Svergun DI, Moradas-Ferreira P, Damas AM (2006) The crystal and solution structures of glyceraldehyde-3-phosphate dehydrogenase reveal different quaternary structures. J Biol Chem 281(44):33433–33440
Fothergill-Gilmore LA, Michels PA (1993) Evolution of glycolysis. Prog Biophys Mol Biol 59(2):105–235
France RM, Grossman SH (2000) Acrylamide quenching of apo- and holo-alpha-lactalbumin in guanidine hydrochloride. Biochem Biophys Res Commun 269(0006-291X (Print)):709–712
Frayne J, Taylor A, Cameron G, Hadfield AT (2009) Structure of insoluble rat sperm glyceraldehyde-3-phosphate dehydrogenase (GAPDH) via heterotetramer formation with Escherichia coli GAPDH reveals target for contraceptive design. J Biol Chem 284(34):22703–22712
Ganapathy-Kanniappan S et al (2009) Glyceraldehyde-3-phosphate dehydrogenase (GAPDH) is pyruvylated during 3-bromopyruvate mediated cancer cell death. Anticancer Res 29(12):4909–4918
Ganapathy-Kanniappan S, Kunjithapatham R, Geschwind JF (2013) Anticancer efficacy of the metabolic blocker 3-bromopyruvate: specific molecular targeting. Anticancer Res 33(1):13–20
Goodsell DS, Morris GM, Olson AJ (1996) Automated docking of flexible ligands: applications of AutoDock. J Mol Recognit 9(1):1–5
Harris JI, Waters M (1976) 1 Glyceraldehyde-3-phosphate dehydrogenase. Enzymes 13:1–49
Hoagland VD Jr, Teller DC (1969) Influence of substrates on the dissociation of rabbit muscle D-glyceraldehyde 3-phosphate dehydrogenase. Biochemistry 8(2):594–602
Jenkins JL, Tanner JJ (2006) High-resolution structure of human D-glyceraldehyde-3-phosphate dehydrogenase. Acta Crystallogr D Biol Crystallogr 62(Pt 3):290–301
Krebs EG (1955) Glyceraldehyde-3-phosphate dehydrogenase from yeast. Methods Enzymol 1:407–411
Lakatos S, Zavodsky P (1976) The effect of substrates on the association equilibrium of mammalian D-glyceraldehyde 3-phosphate dehydrogenase. FEBS Lett 63(1):145–148
Laskowski RA, Hutchinson EG, Michie AD, Wallace AC, Jones ML, Thornton JM (1997) PDBsum: a web-based database of summaries and analyses of all PDB structures. Trends Biochem Sci 22(12):488–490
Luthy R, Bowie JU, Eisenberg D (1992) Assessment of protein models with three-dimensional profiles. Nature 356(6364):83–85. https://doi.org/10.1038/356083a0
Mas-Coma S, Funatsu IR, Bargues MD (2001) Fasciola hepatica and lymnaeid snails occurring at very high altitude in South America. Parasitology 123(Suppl):S115–S127
Mazzola JL, Sirover MA (2001) Reduction of glyceraldehyde-3-phosphate dehydrogenase activity in Alzheimer's disease and in Huntington's disease fibroblasts. J Neurochem 76(2):442–449
Möller M, Denicola A (2002) Protein tryptophan accessibility studied by fluorescence quenching. Biochem Mol Biol Educ 30(3):175–178. https://doi.org/10.1002/bmb.2002.494030030035
Nelson D, Goldstein JM, Boatright K, Harty DWS, Cook SL, Hickman PJ, Potempa J, Travis J, Mayo JA (2001) pH-regulated secretion of a glyceraldehyde-3-phosphate dehydrogenase from Streptococcus gordonii FSS2: purification, characterization, and cloning of the gene encoding this enzyme. J Dent Res 80(1):371–377
Osborne HH, Hollaway MR (1976) An investigation of the nicotinamide-adenine dinucleotide-induced 'tightening' of the structure of glyceraldehyde 3-phosphate dehydrogenase. Biochem J 157(1):255–259
Pathak RK, Baunthiyal M, Shukla R, Pandey D, Taj G, Kumar A (2017) In silico identification of mimicking molecules as defense inducers triggering jasmonic acid mediated immunity against Alternaria blight disease in Brassica species. Front Plant Sci 8:609. https://doi.org/10.3389/fpls.2017.00609
Pawlowski M, Gajda MJ, Matlak R, Bujnicki JM (2008) MetaMQAP: a meta-server for the quality assessment of protein models. BMC Bioinformatics 9:403. https://doi.org/10.1186/1471-2105-9-403
Pettersen EF, Goddard TD, Huang CC, Couch GS, Greenblatt DM, Meng EC, Ferrin TE (2004) UCSF Chimera—a visualization system for exploratory research and analysis. J Comput Chem 25(13):1605–1612
Robert X, Gouet P (2014) Deciphering key features in protein structures with the new ENDscript server. Nucleic Acids Res 42(Web Server issue):W320–W324. https://doi.org/10.1093/nar/gku316
Saunders PA, Chen RW, Chuang DM (1999) Nuclear translocation of glyceraldehyde-3-phosphate dehydrogenase isoforms during neuronal apoptosis. J Neurochem 72(3):925–932
Schultz DE, Hardin CC, Lemon SM (1996) Specific interaction of glyceraldehyde 3-phosphate dehydrogenase with the 5′-nontranslated RNA of hepatitis A virus. J Biol Chem 271(24):14134–14142
Shukla H, Shukla R, Sonkar A, Pandey T, Tripathi T (2017a) Distant Phe345 mutation compromises the stability and activity of Mycobacterium tuberculosis isocitrate lyase by modulating its structural flexibility. Sci Rep 7(1):1058. https://doi.org/10.1038/s41598-017-01235-z
Shukla H, Shukla R, Sonkar A, Tripathi T (2017b) Alterations in conformational topology and interaction dynamics caused by L418A mutation leads to activity loss of Mycobacterium tuberculosis isocitrate lyase. Biochem Biophys Res Commun 490:276–282. https://doi.org/10.1016/j.bbrc.2017.06.036

Shukla R, Shukla H, Tripathi T (2018) Activity loss by H46A mutation in Mycobacterium tuberculosis isocitrate lyase is due to decrease in structural plasticity and collective motions of the active site. Tuberculosis (Edinb) 108:143–150

Singh R, Green MR (1993) Sequence-specific binding of transfer RNA by glyceraldehyde-3-phosphate dehydrogenase. Science 259(5093): 365–368

Sirover MA (1999) New insights into an old protein: the functional diversity of mammalian glyceraldehyde-3-phosphate dehydrogenase. Biochim Biophys Acta 1432(2):159–184

Soares FA, Sesti-Costa R, da Silva JS, de Souza MCBV, Ferreira VF, da C. Santos F, Monteiro PAU, Leitão A, Montanari CA (2013) Molecular design, synthesis and biological evaluation of 1,4-dihydro-4-oxoquinoline ribonucleosides as TcGAPDH inhibitors with trypanocidal activity. Bioorg Med Chem Lett 23(16):4597–4601. https://doi.org/10.1016/j.bmcl.2013.06.029

Van de Weert M, Stella L (2011) Fluorescence quenching and ligand binding: a critical discussion of a popular methodology. J Mol Struct 998(1–3):144–150. https://doi.org/10.1016/j.molstruc.2011.05.023

Webb B, Sali A (2014) Comparative protein structure modeling using MODELLER. Curr Protoc Bioinformatics 47:5 6 1–5 632. https://doi.org/10.1002/0471250953.bi0506s47

WHO (2015) WHO estimates of the global burden of foodborne diseases: foodborne disease burden epidemiology reference group 2007–2015. World Health Organization

Wiederstein M, Sippl MJ (2007) ProSA-web: interactive web service for the recognition of errors in three-dimensional structures of proteins. Nucleic Acids Res 35(Web Server):W407–W410. https://doi.org/10.1093/nar/gkm290

Zinsser VL, Hoey EM, Trudgett A, Timson DJ (2014) Biochemical characterisation of glyceraldehyde 3-phosphate dehydrogenase (GAPDH) from the liver fluke, Fasciola hepatica. Biochim Biophys Acta 1844(4):744–749. https://doi.org/10.1016/j.bbapap.2014.02.008